

## Determination of the Sign of the $K_L^0-K_S^0$ Mass Difference

D. G. Hill, M. Sakitt, and O. Skjeggstad\*  
*Brookhaven National Laboratory, Upton, New York 11973†*

and

J. Canter, ‡ Y. Cho, § A. Dralle, || A. Engler, H. Fisk, R. Kraemer, and C. Meltzer  
*Carnegie-Mellon University, Pittsburgh, Pennsylvania 15213†*

and

T. Kikuchi,\*\* D. K. Robinson, and C. Tilger††  
*Case Western Reserve University, Cleveland, Ohio 44106§§*

(Received 24 March 1971)

The final results of our experiment to measure the sign of the  $K_L^0-K_S^0$  mass difference are presented. The sign has been measured by studying the time distribution of scattered neutral  $K$  mesons, using  $K^0$ 's from the reaction  $K^+ + d \rightarrow K^0 + p + p$ . We obtain  $M_{K_L} > M_{K_S}$ .

### I. INTRODUCTION

The sign of  $\Delta m$ , where  $\Delta m \equiv M_{K_L} - M_{K_S}$ , plays an important role in the phenomenology of  $CP$  non-invariance in neutral  $K$  decay. The phase of  $\epsilon$ , which is a measure of the extent to which  $K_S$  and  $K_L$  are not eigenstates of  $CP$ , is related to  $\Delta m$  through the equation

$$\arg \epsilon \approx 2\Delta m / \Gamma_S = 43^\circ,$$

where contributions from leptonic,  $3\pi$ , and  $2\pi$  ( $I=2$ ) final states have been neglected.  $\Gamma_S$  is the  $K_S$  decay rate.

Several experiments to determine the sign of  $\Delta m$  have been reported.<sup>1-4</sup> They yield, with varying degrees of confidence, a positive sign of  $\Delta m$ . The main feature of these experiments is a measurement of the  $K_S^0 \rightarrow \pi^+\pi^-$  intensity resulting from the interference of transmitted and regenerated (or scattered)  $K_S^0$  mesons. The experimental observation of such an interference term, together with a knowledge of the scattering amplitudes, allows the determination of the sign of  $\Delta m$ .

In this experiment we used the method proposed by Camerini, Fry, and Gaidos.<sup>5</sup> If a pure  $K^0$  state is produced at  $t=0$ , undergoes nuclear scattering at time  $t$ , and then the  $K_S^0$  state is observed to decay at time  $t'$ , the intensity of scattering as a function of  $t$  will depend on  $\sin(\Delta m t)$ . Preliminary results from this experiment<sup>†</sup> showed that the sign of  $\Delta m$  is positive. Since that time, additional data have been accumulated and more information concerning scattering amplitudes has become available. The final results from the experiment, with details concerning the use of the results of published phase-shift analyses, are reported here.

### II. THEORY

In 1963, Camerini, Fry, and Gaidos<sup>5</sup> suggested that the sign of  $\Delta m$  could be determined by the analysis of the time distribution of elastic scatters of neutral  $K$  mesons, followed by their decay via the short-lived state into the  $\pi^+\pi^-$  mode. To the statistical accuracy of our experiment, we can neglect the small  $CP$ -nonconserving effects and define

$$|K_S^0\rangle = (|K^0\rangle + |\bar{K}^0\rangle) / \sqrt{2}$$

and

$$|K_L^0\rangle = (|K^0\rangle - |\bar{K}^0\rangle) / \sqrt{2},$$

with the convention  $CP|K^0\rangle = |\bar{K}^0\rangle$ .

Assuming at time  $t=0$  a  $K^0$  is produced, then

$$|\psi(0)\rangle = |K^0\rangle = (|K_S^0\rangle + |K_L^0\rangle) / \sqrt{2}.$$

At a later time  $t$ , the amplitude evolves into

$$|\psi(t)\rangle = \frac{1}{2} [(|K^0\rangle + |\bar{K}^0\rangle)e^{-i\omega_S t} + (|K^0\rangle - |\bar{K}^0\rangle)e^{-i\omega_L t}],$$

where  $\omega_{S,L} = M_{K_{S,L}} - \frac{1}{2}i\lambda_{S,L}$ .  $\lambda_S$  and  $\lambda_L$  are the decay rates for the short-lived and long-lived decay modes. If an elastic scatter occurs at time  $t$ , the amplitude becomes

$$|\psi_{sc}(t)\rangle = \frac{1}{2} [(f|K^0\rangle + \bar{f}|\bar{K}^0\rangle)e^{-i\omega_S t} + (f|K^0\rangle - \bar{f}|\bar{K}^0\rangle)e^{-i\omega_L t}],$$

where  $f$  and  $\bar{f}$  are the  $KN$  and  $\bar{K}N$  scattering amplitudes, respectively. The  $K_S$  amplitude at time  $t$  is then given by

$$\langle K_S^0 | \psi_{sc}(t) \rangle = \frac{1}{2\sqrt{2}} [(f + \bar{f})e^{-i\omega_S t} + (f - \bar{f})e^{-i\omega_L t}].$$

This expression explicitly shows the  $K_S$  amplitude as a coherent sum of two parts, each of which has a simple physical interpretation. The first part is the original  $K_S$  amplitude after nuclear scattering, while the second part is a  $K_S$  amplitude regenerated in the scattering from the original  $K_L$  component. Experimentally one observes the time distribution of  $K_S$  decays at time  $t'$ , following the scattering which occurred at time  $t$ , given by

$$F(t, t', \Delta m) = |\langle K_S^0 | \psi_{sc}(t) \rangle e^{-i\omega_S t'}|^2. \quad (1)$$

In the conventional way, we let  $f = A + A' \vec{\sigma} \cdot \hat{n}$  and  $\bar{f} = B + B' \vec{\sigma} \cdot \hat{n}$ , where  $A$  and  $B$  are the non-spin-flip amplitudes, and  $A'$  and  $B'$  are the spin-flip amplitudes. Then we can rewrite Eq. (1) as

$$F(t, t', \Delta m) = I(t, \Delta m) e^{-\lambda_S t'},$$

where

$$\begin{aligned} I(t, \Delta m) = & \frac{1}{8} [ (|A+B|^2 + |A'+B'|^2) e^{-\lambda_S t} \\ & + (|A-B|^2 + |A'-B'|^2) e^{-\lambda_L t} \\ & + 2(|A|^2 - |B|^2 + |A'|^2 - |B'|^2) e^{-\Lambda t} \cos(\Delta m t) \\ & - 4(\text{Im } A^* B + \text{Im } A'^* B') e^{-\Lambda t} \sin(\Delta m t) ] \end{aligned} \quad (2)$$

and

$$\Lambda = \frac{1}{2}(\lambda_S + \lambda_L).$$

In this particular experiment, the neutral  $K$  scatterers on deuterium, giving rise to four possible elastic reactions. These reactions, with their related isotopic-spin amplitudes, are listed below; the subscript refers to the isotopic spin.

$$K^0 + p \rightarrow K^0 + p: \frac{1}{2}(A_1 + A_0), \frac{1}{2}(A'_1 + A'_0),$$

$$K^0 + n \rightarrow K^0 + n: A_1, A'_1,$$

$$\bar{K}^0 + p \rightarrow \bar{K}^0 + p: B_1, B'_1,$$

$$\bar{K}^0 + n \rightarrow \bar{K}^0 + n: \frac{1}{2}(B_1 + B_0), \frac{1}{2}(B'_1 + B'_0).$$

The development of Eq. (2), however, ignores any spin and binding effects caused by the deuterium target. That is, the impulse approximation has been assumed to be valid and the scattering process has been treated as in the free-target case. Elastic scattering on the whole deuteron is treated separately in Sec. IV. The isotopic-spin amplitudes, which have been deduced from measurements of  $K^+$  and  $K^-$  scattering by hydrogen and deuterium (see Sec. IV), are functions of the center-of-mass momentum  $k$  and the center-of-mass scattering angle  $\theta$ , and are parametrized in a standard partial-wave manner. Accordingly, the  $KN$  non-spin-flip and spin-flip amplitudes are

$$A_I = \frac{1}{k} \sum_l [(l+1) T_{l+1/2}^I + l T_{l-1/2}^I] P_l(\cos \theta)$$

and

$$A'_I = \frac{i}{k} \sum_l [T_{l+1/2}^I - T_{l-1/2}^I] P_l^I(\cos \theta),$$

where  $I$  is the isotopic spin,  $l$  is the orbital angular momentum,  $P_l(\cos \theta)$  and  $P_l^I(\cos \theta)$  are the Legendre polynomials and associated Legendre polynomials, respectively, and  $T$  is a partial-wave amplitude. Similar expressions hold for the  $\bar{K}N$  amplitudes  $B$  and  $B'$ . Discussion of the partial-wave amplitudes used in our analysis is found in Sec. IV A.

### III. EXPERIMENTAL PROCEDURE

#### A. Exposure

The events were obtained from the 30-in. BNL bubble chamber, filled with deuterium, exposed to a separated 600-MeV/c  $K^+$  beam<sup>6</sup> at the Alternating Gradient Synchrotron (AGS). In the first part of the exposure, 250 000 pictures were obtained with an average flux of 13  $K^+$  per picture and an equal number of background tracks. For the second part, 500 000 additional pictures were obtained with an average flux of 25  $K^+$  and about two background tracks per picture. Neutral  $K$  mesons were produced in the  $K^0$  state via the reaction

$$K^+ + d \rightarrow K^0 + p + p_S, \quad (3)$$

where  $p_S$  is a spectator proton.

#### B. Scanning and Measuring

The entire exposure was scanned for  $V$ 's, regardless of origin. Every  $V$  found in the scan was measured together with the most likely (usually the closest)  $K^0$  production vertex, and these events were processed through geometry and kinematics programs standard to each of the participating groups of experimenters. All events which fitted the normal production sequence,  $K^+ + d \rightarrow K^0 + p + p_S$ , followed by decay,  $K^0 \rightarrow \pi^+ + \pi^-$ , with an over-all  $\chi^2$  probability greater than 0.001, were assumed to be direct  $K^0$  production followed by two-body decay. For the purposes of this experiment, these events were excluded from further analysis. Approximately 50 000 such events were found. The only competing production reactions are

$$K^+ + d \rightarrow K^0 + p + \pi^0 + p_S \quad (4)$$

and

$$K^+ + d \rightarrow K^0 + n + \pi^+ + p_S. \quad (5)$$

The combined total cross section for such production is  $\sim 0.1$  mb at 600 MeV/c, relative to 6.5 mb for the reaction (3); (4) is easily distinguished kinematically, and (5) visually, from (3). Such productions were eliminated. Each event which failed the normal sequence was examined on the scan table with the kinematic information at hand. If the failure to make the normal fit was due to an incorrect choice of production vertex or other mis-measurement, the event was remeasured as nec-

essary until it could be classified.

Events which fit the decay hypothesis  $K^0 \rightarrow \pi^+ + \pi^-$  with the  $K^0$  direction unknown (1c fit), but did not make a 3c fit to any production vertex, were classified as scattered  $K$  candidates. These were examined for possible associated proton recoil tracks using the known direction of flight of the decaying  $K_S^0$ . Each was measured with all possible recoil proton tracks and production vertices, and fitted to the sequences

$$\begin{aligned} K^+ + d &\rightarrow K^0 + p + p_S \quad (\text{production}), \\ K^0 + d &\rightarrow K^0 + n + p \quad (\text{breakup}), \\ K^0 &\rightarrow \pi^+ + \pi^- \quad (K_S^0 \text{ decay}), \end{aligned} \quad (6)$$

and

$$\begin{aligned} K^+ + d &\rightarrow K^0 + p + p_S \quad (\text{production}), \\ K^0 + d &\rightarrow K^0 + d \quad (\text{whole deuteron}), \\ K^0 &\rightarrow \pi^+ + \pi^- \quad (K_S^0 \text{ decay}). \end{aligned} \quad (7)$$

#### C. Event Selection

To guarantee a sample of data which is free of time bias, both geometrical and kinematical selection criteria were imposed:

- (a) The three vertices (production, recoil, and decay) had to lie within a cylindrical volume of 30-cm radius and 25-cm height, centered in the bubble chamber.
- (b) The magnitude of the dip angle of the scattered  $K$ , of the charged recoil, and of the  $\pi^+$  and  $\pi^-$  had to be less than  $70^\circ$ .
- (c) The  $K^0$  momentum from the  $K_S^0 \rightarrow \pi^+ \pi^-$  fit had to be greater than 200 MeV/c and less than 600 MeV/c.
- (d) The projected length of the charged recoil had to be greater than 0.2 cm.
- (e) The projected distance from the recoil vertex to the  $K_S^0$  decay had to be greater than 0.1 cm.
- (f) The distance from production to recoil vertex had to be greater than 0.6 cm.
- (g) The length from  $K^0$  production to recoil vertex had to be less than 20 cm.

Possible time biases at short neutral track lengths [cuts (e) and (f)] and small scattering angle [cut (d)] were investigated by varying these cuts and looking for shifts in the results. None were found.

Since we observe  $K_S \rightarrow \pi^+ + \pi^-$ , the sample of  $K_S$  should have a lifetime in agreement with the known  $K_S$  lifetime. A maximum-likelihood analysis of our total sample of 175 events yields a lifetime of  $(0.80 \pm 0.07) \times 10^{-10}$  sec, in agreement with the present world average of  $(0.862 \pm 0.006) \times 10^{-10}$  sec.<sup>7</sup>

#### D. Event Classification

Two classes of  $K$  scatters are expected in deute-

rium: those events where the scatter occurs on one nucleon with the other nucleon as a spectator [sequence (6)], and those events where the whole deuteron recoils [sequence (7)]. Nearly every event that fitted the whole-deuteron sequence also fitted the breakup sequence. In spite of this fitting overlap, we were able clearly to isolate the whole-deuteron events, and can demonstrate a reasonable good division of the remaining events into neutron and proton scatters.

#### 1. Whole-Deuteron Scatters

In Fig. 1 the cosine of the space angle between the two nucleons, from the fit to the breakup reaction, is plotted. To the extent that one can neglect the variation of cross section with center-of-mass energy, one expects the orientation of the spectator nucleon to be approximately random. Then the cosine of the angle between the outgoing target nu-

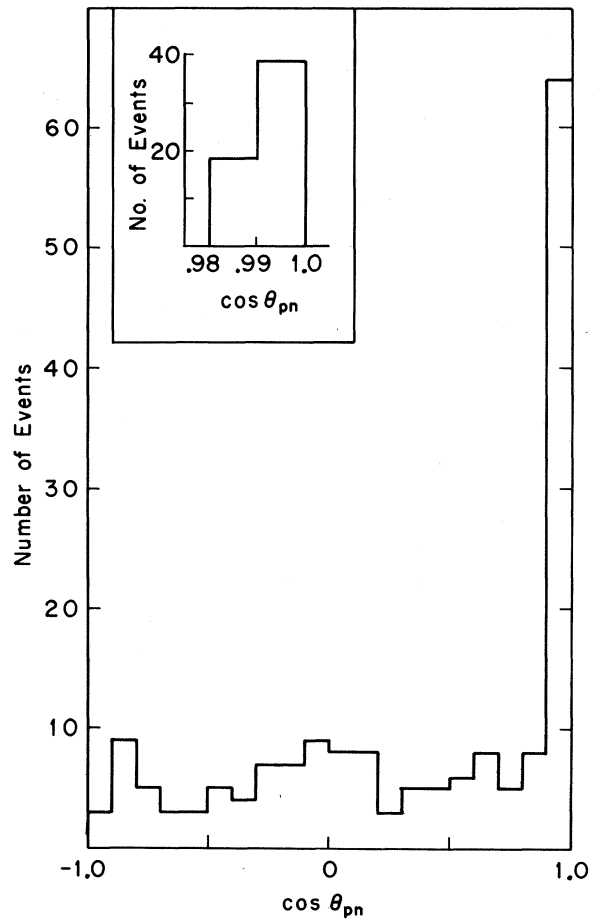


FIG. 1. Plot of the distribution in the cosine of the space angle (interval 0.1) between the two nucleons in the fit to the breakup reaction. Deuteron events are classified as those having  $\cos \theta_{pn} > 0.98$ . These 56 events are also shown in the inset.

cleon and the spectator nucleon would be isotropic for those events where the deuteron breaks up. On the other hand, for an event where the deuteron remains whole, the momentum transfer of the neutral  $K$  is along the direction of the charged recoil, and in the fit to the breakup reaction the neutron would be forced to line up along the proton. We have classified as whole-deuteron events those in Fig. 1 having  $\cos\theta_{pn} > 0.98$ . There are 56 such events which include approximately one true breakup reaction. These whole-deuteron events are analyzed in Sec. V B.

### 2. Neutron and Proton Scatters

There now remains the division of breakup scatters into neutron and proton events. Figure 2 is a scatter plot of the fitted neutron vs fitted proton momentum for the 133 events remaining after the deuteron scatters have been removed. For most of the data, the distinction between target and spectator nucleon is clear. However, to increase the reliability of the separation, additional selection criteria have been imposed. All scatters where the magnitude of the difference in momenta of the outgoing nucleons is less than 30 MeV/c have been removed. This amounts to 11 events in the 45° band of Fig. 2. Also, three events where both outgoing nucleons had momenta greater than 300 MeV/c have been cut. The remaining breakup events were then classified by assuming the scatter occurred on the nucleon with the higher momentum. With this separation procedure, we found 78 scatters on protons and 41 scatters on neutrons.

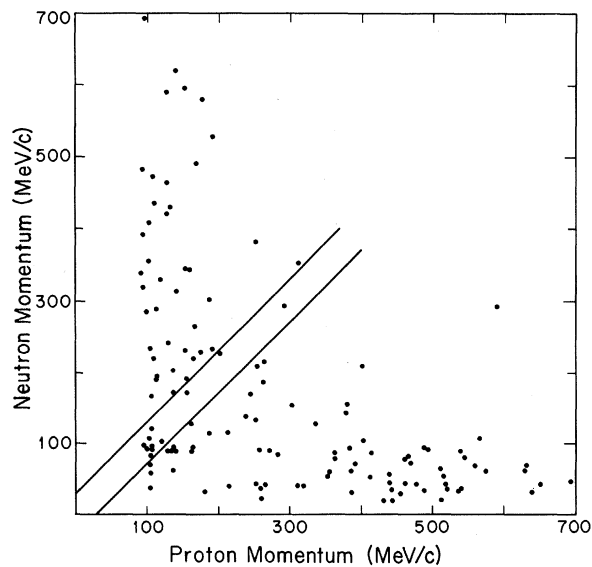


FIG. 2. Scatter plot of proton momentum versus neutron momentum in the laboratory for the reaction  $(\bar{K}^0, K^0) + d \rightarrow (\bar{K}^0, K^0) + p + n$ .

When the spectator momentum distributions are compared with the Hulthén wave-function predictions, reasonable agreement is found, as shown in Figs. 3(a) and 3(b).

## IV. SCATTERING AMPLITUDES

### A. General

The laboratory momentum spectrum of the incident neutral  $K$ 's for the breakup events is shown in Fig. 4(a), with the corresponding plot for the whole-deuteron scatters shown in Fig. 4(b). The scattering amplitudes of  $K^0$  and  $\bar{K}^0$  on neutrons and protons in the momentum region between 200 and 600 MeV/c have been deduced, assuming charge independence, from  $K^+$  and  $K^-$  scattering

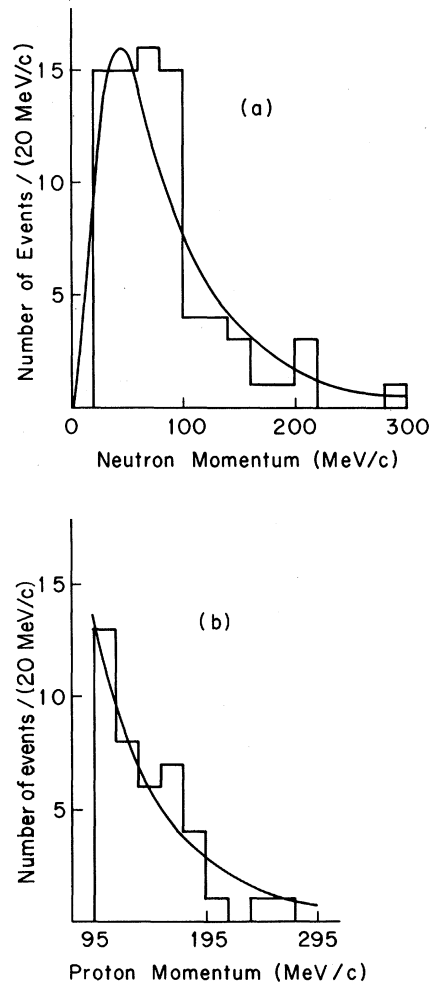


FIG. 3. (a) Spectator neutron momentum distribution for 78 proton scatters, (b) Spectator proton momentum distribution for 41 neutron scatters. The momenta are in the laboratory system and the solid curves are the normalized Hulthén distributions.

data in hydrogen and deuterium.<sup>8-15</sup> Scattering amplitudes for each event have been constructed from the isotopic-spin amplitudes as given in Sec. II. The center-of-mass momentum and scattering angle for each event were computed with the assumption that the momentum of the target nucleon before interaction was equal in magnitude but opposite in direction to the spectator nucleon.

#### B. $K$ -Nucleon Amplitudes

The  $K^+$ -nucleon interaction has been investigated in detail and has been found to be predominantly elastic at momenta up to 800 MeV/c. Therefore one parametrizes the  $KN$   $I=0$  and  $I=1$  partial-wave amplitudes,  $T_J^I$ , in the standard form:

$$T_J^I = \frac{e^{2i\delta_J^I} - 1}{2i},$$

where  $I$  is the isotopic spin,  $J = l \pm \frac{1}{2}$ , and  $\delta_J^I$  is the phase shift which contains the momentum-dependence.

The  $I=1$   $KN$  amplitude, determined from  $K^+p$  scattering data,<sup>8</sup> can be well described by a dominant S-wave amplitude. Constructive interference between this amplitude and the Coulomb amplitude has been observed at the low momenta. Therefore we parametrize the  $I=1$   $KN$  elastic scattering by a negative S-wave phase shift,  $\delta_0^1$ , which decreases

linearly with increasing incident- $K$  center-of-mass momentum. Figure 5 shows the experimental data that exist on  $\delta_0^1$ , with the solid curve representing the above linear approximation.

The  $I=0$   $KN$  amplitude, in the momentum region from 230 to 800 MeV/c, has been investigated by Slater *et al.*<sup>9</sup> and by Stenger *et al.*,<sup>10</sup> and at 600 MeV/c by Ray *et al.*<sup>16</sup> Stenger *et al.* studied  $K^+n$  elastic and charge-exchange scattering (mixtures of  $I=0$  and  $I=1$ ) with a phase-shift analysis which used fixed  $I=1$  amplitudes determined from  $K^+p$  data. Good solutions were found with  $S$  and  $P$ , or  $S$ ,  $P$ , and  $D$  waves, for the  $I=0$  amplitude. The  $SP$  and  $SPD$  solutions contain a Fermi-Yang ambiguity; the  $SPa$  and  $SPDa$  Fermi solutions are characterized by dominant  $p_{3/2}$  phase shifts, and the  $SPb$  and  $SPDb$  Yang solutions have dominant  $P_{1/2}$  phase shifts. This Fermi-Yang ambiguity was resolved by Ray *et al.*<sup>16</sup> in a measurement of the recoil-proton polarization in the reaction  $K^+ + n \rightarrow K^0 + p$  at an incident  $K^+$  laboratory momentum of 600 MeV/c. The  $SPb$  and  $SPDb$  (Yang-type) solutions were highly favored. These solutions were also favored in an over-all fit to existing  $K^+p$  and  $K_L^0p$  data.<sup>17</sup> In our analysis, we use  $SPDb$  as the preferred solution, although the exclusion of  $D$  waves has an almost indiscernible effect. We have parametrized the  $I=0$   $SPDb$  phase shifts as a power series in  $k$ , the center-of-mass momentum, and have included terms up to  $k^4$ . This parametrization is shown in Fig. 6 as a solid curve, along with the experimentally determined points from the

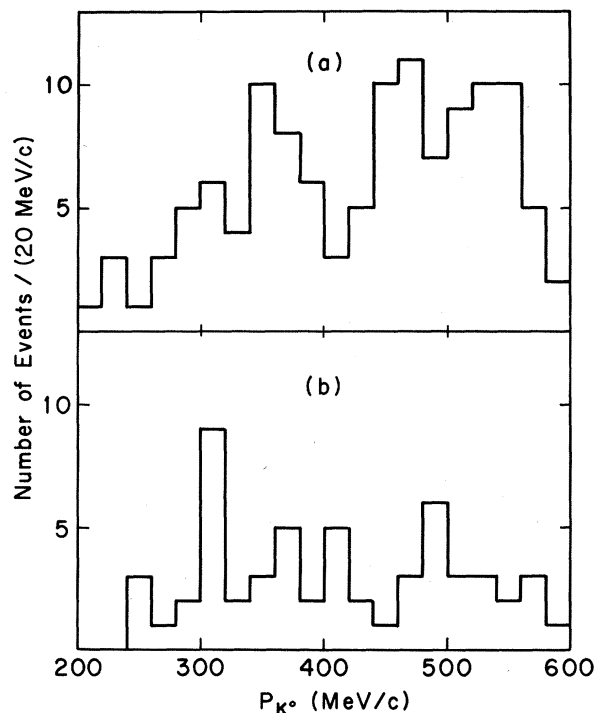


FIG. 4. Momentum distribution of  $K^0$ 's incident at the scattering vertex: (a) for 119 breakup events and (b) for 56 whole-deuteron events.

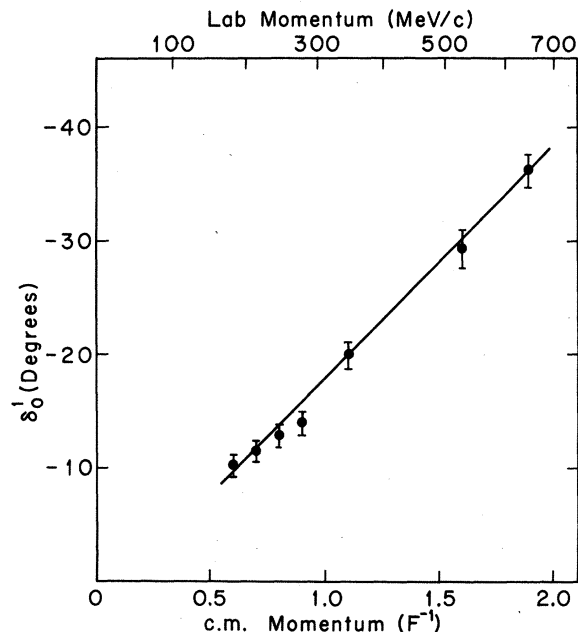


FIG. 5.  $I=1$   $K$ -nucleon S-wave phase-shift parametrization. The data are from Ref. 8.

SPDb solution.

### C. $\bar{K}$ -Nucleon Amplitudes

Unlike the  $K$ -nucleon reaction, the  $\bar{K}$ -nucleon interaction is highly inelastic over the entire momentum region of interest. At the lower momentum region,  $K^-p$  interactions have been studied by Humphrey and Ross,<sup>11</sup> Sakitt *et al.*,<sup>12</sup> and Kim.<sup>13</sup> A multichannel analysis on available experimental data for all channels of  $K^-p$  and  $K^-n$  interactions, in the  $K^-$  laboratory momentum range 0 to 550 MeV/c, was performed by Kim<sup>18</sup> using the effective-range parametrization of Ross and Shaw.<sup>19</sup> More recently, Armenteros *et al.*<sup>14</sup> have studied  $K^-p$  interactions in the momentum region 430 to 800 MeV/c.

We use the multichannel solution of Kim in the region 100 to 430 MeV/c, and the parametrization of Armenteros *et al.* in the region 430 to 600 MeV/c. Each of these regions is discussed in detail below.

#### 1. 100 to 430 MeV/c

In this region the scattering amplitudes are dominated by two-body final states, and this feature allows the use of the multichannel effective-range formalism in determining the scattering amplitudes. In this formalism, the partial-wave amplitude,  $T$ , is generalized to a transition matrix,  $\mathcal{T}$ , whose elements  $\mathcal{T}_{nm}$  correspond to a scat-

tering amplitude from the initial state  $n$  to the final state  $m$ . Elastic scattering corresponds to the  $\mathcal{T}_{11}$  matrix element. The transition matrix is written in terms of a real, symmetric matrix  $\mathfrak{M}$ , as

$$\mathcal{T}_I^J = \rho^{I+1/2} (\mathfrak{M}_I^J - \rho^{2I+1})^{-1} \rho^{I+1/2},$$

where  $\rho^{I+1/2}$  is a diagonal phase-space matrix with elements  $k_m^{I+1/2}$ .  $k_m$  is the center-of-mass momentum of the  $m$ th channel and  $l_m$  is the orbital angular momentum in that channel. In the effective-range theory, the matrix  $\mathfrak{M}$  is expanded about the  $\bar{K}N$  threshold ( $E_0$ ), so that for an energy  $E$  we have

$$\mathfrak{M}_I^J(E) = \mathfrak{M}_I^J(E_0) + \frac{1}{2} \mathcal{R}_I^J [k^2(E) - k^2(E_0)].$$

In the approximation used by Kim,  $\mathcal{R}$  was taken to be an energy-independent diagonal matrix of effective ranges with the property that the elements

$$\mathcal{R}_{nm} = C_{in} \gamma_{nm}^{1-2I},$$

TABLE I. Results of the multichannel effective-range analysis of Ref. 18.  $\mathfrak{M}_{nm}^I$  is the  $\mathfrak{M}$ -matrix element for isospin  $I$ , and  $n$  and  $m$  are the initial and final channels.  $\mathcal{R}_{nm}^I$  is the channel effective range.  $a_1$  and  $b_1$  are the real and imaginary parts of the  $D_3^1$  scattering length, and  $E_r$ ,  $\Gamma$ , and  $\Gamma_K$  are the parameters of the  $D_3^0$  resonance.  $\mathfrak{M}$  is in units of  $F^{-(2I+1)}$  and  $\mathcal{R}$  is in  $F$ .

	$S_1$	$P_1$	$P_3$
$\mathfrak{M}_{KK}^0$	$0.00 \pm 0.02$	$17.5 \pm 16.4$	$10.9 \pm 0.9$
$\mathfrak{M}_{K\Sigma}^0$	$-1.11 \pm 0.04$	$-10.6 \pm 4.5$	$-1.4 \pm 0.2$
$\mathfrak{M}_{\Sigma\Sigma}^0$	$2.04 \pm 0.10$	$-11.4 \pm 4.8$	$5.6 \pm 0.5$
$\mathfrak{M}_{KK}^1$	$-3.60 \pm 0.02$	$-18.1 \pm 0.7$	$5.2 \pm 1.0$
$\mathfrak{M}_{K\Sigma}^1$	$-2.86 \pm 0.03$	$7.2 \pm 1.1$	$-13.8 \pm 1.6$
$\mathfrak{M}_{K\Lambda}^1$	$2.08 \pm 0.07$	$4.7 \pm 0.4$	$-11.9 \pm 1.6$
$\mathfrak{M}_{\Sigma\Sigma}^1$	$-1.40 \pm 0.06$	$-0.3 \pm 1.1$	$-15.8 \pm 0.9$
$\mathfrak{M}_{\Sigma\Lambda}^1$	$1.81 \pm 0.04$	$-6.8 \pm 1.0$	$-13.6 \pm 0.2$
$\mathfrak{M}_{\Lambda\Lambda}^1$	$-2.31 \pm 0.11$	$-3.4 \pm 1.3$	$-16.3 \pm 2.0$
$\mathcal{R}_{KK}^0$	$0.54 \pm 0.08$	...	...
$\mathcal{R}_{\Sigma\Sigma}^0$	$-0.89 \pm 0.31$	...	...
$\mathcal{R}_{KK}^1$	$-0.13 \pm 0.07$	...	$-0.66 \pm 0.20$
$\mathcal{R}_{\Sigma\Sigma}^1$	$-0.78 \pm 0.23$	...	$0.27 \pm 0.05$
$\mathcal{R}_{\Lambda\Lambda}^1$	$-1.22 \pm 0.45$	...	$0.31 \pm 0.13$
$D_3^1$ (zero effective range)		$D_3^0$ (Breit-Wigner resonance)	
$a_1$	$0.006 \pm 0.003 F^5$	$E_r$	$1518.8 \pm 0.7 \text{ MeV}$
$b_1$	$0.002 \pm 0.001 F^5$	$\Gamma$	$16.2 \pm 1.0 \text{ MeV}$
		$\Gamma_K$	$0.45\Gamma \text{ MeV}^a$

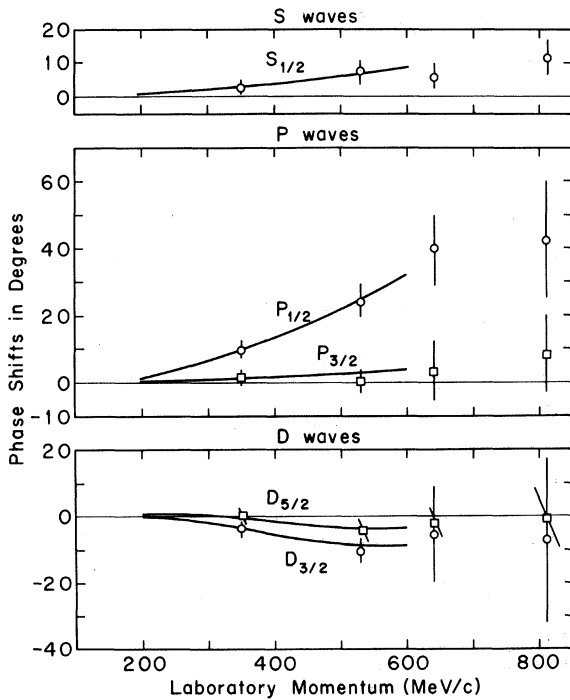


FIG. 6.  $I=0$   $K$ -nucleon phase-shift parametrization. The data are from Ref. 10.

<sup>a</sup>We have used  $\Gamma_K = 0.45\Gamma$  in our analysis.

where  $C_{0n}=1$  for  $S$  waves,  $C_{1n}=-3$  for  $P$  waves, and  $\gamma_{nm}$  are the fitted ranges.

Since the  $I=0$  scattering has two channels, the  $\bar{K}N$  and  $\Sigma\pi$ , and the  $I=1$  scattering has three channels, the  $\bar{K}N$ ,  $\Sigma\pi$ , and  $\Lambda\pi$ , the  $S$ -wave scattering is described by nine matrix elements and five effective ranges. The  $P$ -wave scattering is not large enough to yield a meaningful range except in the case of  $I=1$ ,  $P_{3/2}$ . Thus, there are only nine  $P_{1/2}$  matrix elements, while the  $P_{3/2}$  has nine matrix elements plus three effective ranges. The  $D$ -wave resonant state  $\Lambda(1520)$  is parametrized by a Breit-Wigner form. Table I lists the parameters, extracted from the work of Kim,<sup>18</sup> which were used in our analysis.

## 2. 430 to 600 MeV/c

The  $\bar{K}$ -nucleon amplitudes in this momentum region were taken from the analysis of Armenteros *et al.*<sup>14</sup> who studied the two-body final states from 430 to 800 MeV/c. The authors performed an energy-dependent partial-wave analysis and found their parametrization connected continuously to results at both higher and lower energies. Their result is that the  $\bar{K}N$  channel, between 430 and 600 MeV/c, can be adequately described by  $S$ - and  $P$ -wave nonresonant amplitudes of the form

$$r_i^j = a_i^j + b_i^j(p - 0.6),$$

where  $p$  is the laboratory momentum of the kaon in GeV/c, and  $a$  and  $b$  are complex parameters. The  $D$ -wave state  $\Lambda(1520)$  was assumed to be a Breit-Wigner form. Table II lists the parameters of interest extracted from Ref. 14.

### D. Scattered $K_S^0$ Intensity Distribution

The result of this experiment depends on constructive interference between the scattered and regenerated  $K_S$  amplitudes in the time interval  $\tau_S$  to  $4\tau_S$ , where  $\tau_S$  is the  $K_S$  lifetime. The main characteristics of the scattering amplitudes are listed below:

- (a) The  $S$  waves dominate and the spin-flip am-

plitudes are small compared to non-spin-flip amplitudes.

(b) The  $\bar{K}^0N$  amplitudes ( $B$ ) are predominantly imaginary and positive.

(c) The  $K^0N$  amplitudes ( $A$ ) are predominantly real and negative.

(d) The  $\bar{K}^0N$  cross sections are larger than those of  $K^0N$ .

Examination of the intensity distribution, Eq. (2), shows that the term  $[|A|^2 - |B|^2]$  is negative while the term  $[-4 \text{Im}(A^*B)]$  is positive. These rough conclusions concerning the signs of these coefficients are, in fact, true in the laboratory momentum range 200–600 MeV/c for scatters off neutrons and protons at nearly all scattering angles. It is then easy to understand the shape of the time distribution; the four terms and their resulting sum are shown in Figs. 7(a) and 7(b) for neutron scatters at 400 MeV/c and center-of-mass angle  $60^\circ$ . For  $M_{KL} > M_{KS}$  a broad enhancement is expected in the region  $\tau_S$  to  $4\tau_S$ , but for  $M_{KS} > M_{KL}$  almost complete destructive interference is expected near  $t = \tau_S$ .

## V. RESULTS

### A. Nucleon Events

For the  $i$ th event, which was classified as either a neutron or proton scatter, we constructed the scattering amplitudes  $A_i$ ,  $B_i$ ,  $A'_i$ ,  $B'_i$ , using the fitted  $K^0$  momentum and scattering angle and the general amplitude parametrization described in the previous section. Then a likelihood function for the 119 nucleon events was defined by

$$L(\Delta m) = \prod_{i=1}^N \frac{I_i(t_i, \Delta m)}{\int_{t_i^{\min}}^{t_i^{\max}} I_i(t, \Delta m) dt},$$

where  $t_i$  is the time of the scatter of the  $i$ th event,  $N$  is the number of events, 119, and  $t_i^{\min}$  and  $t_i^{\max}$  are the times which correspond to the minimum and maximum observable distances for that event in the chamber, as determined by the geometrical

TABLE II. Results of the partial-wave analysis of Ref. 14.

Amplitude	Rea	Ima	Reb	Imb
$S_1^0$	$0.19 \pm 0.05$	$0.78 \pm 0.02$	$1.33 \pm 0.48$	$0.04 \pm 0.25$
$S_1^1$	$0.05 \pm 0.04$	$0.38 \pm 0.02$	$0.29 \pm 0.50$	$0.05 \pm 0.27$
$P_1^0$	$0.17 \pm 0.05$	$0.12 \pm 0.03$	$-0.48 \pm 0.39$	$0.34 \pm 0.43$
$P_1^1$	$-0.07 \pm 0.05$	$0.05 \pm 0.02$	$-0.60 \pm 0.66$	$-0.38 \pm 0.33$
$P_3^0$	$0.27 \pm 0.03$	$0.11 \pm 0.01$	$0.62 \pm 0.33$	$0.15 \pm 0.30$
$P_3^1$	$0.00 \pm 0.03$	$0.07 \pm 0.01$	$-0.13 \pm 0.28$	$0.43 \pm 0.08$

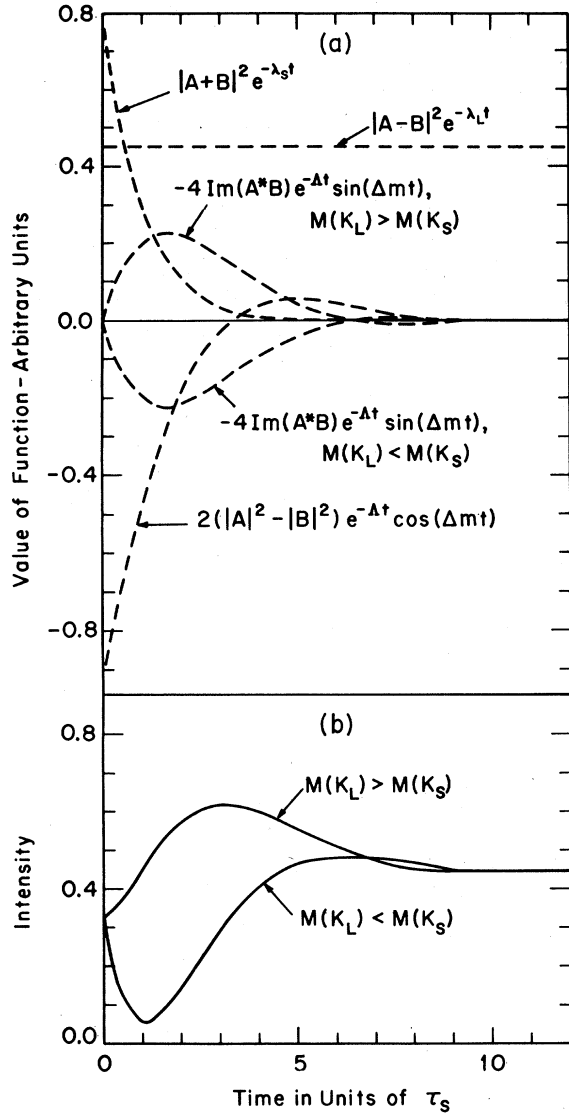


FIG. 7. (a) Plot of the four terms of Eq. (2) as a function of time for neutron scatters at 400 MeV/c and center-of-mass angle  $60^\circ$ . Contributions from terms containing  $A'$  and  $B'$  are also included in the plot, but the labels do not include those terms for convenience only. (b) The sum of the four terms of Eq. (2) for both  $M_{K_L} > M_{K_S}$  and  $M_{K_S} > M_{K_L}$ .

cuts described in Sec. III. The notation  $I_i$  refers to the fact that each event was described by different scattering amplitudes and therefore a different intensity function. A plot of the likelihood function is shown in Fig. 8, with the arrow corresponding to the accepted value<sup>7</sup> of  $|\Delta m| = (0.469 \pm 0.015)\tau_s^{-1}$ . We observe a maximum at

$$M_{K_L} - M_{K_S} = +(0.58 \pm 0.12)\tau_s^{-1},$$

in excellent agreement with the known magnitude of the mass difference. There is a local maximum

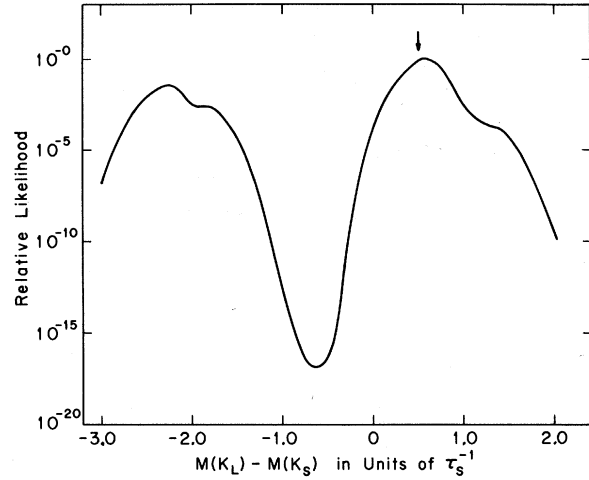


FIG. 8. Plot of the relative likelihood function of  $\Delta m = M(K_L) - M(K_S)$  for 119 breakup events. The arrow shows the accepted value of  $|\Delta m|$ .

near  $\Delta m = -2.3$  which is completely excluded by the measurement of the magnitude. We have analyzed the data with alternate scattering amplitudes, and have also examined the proton and neutron samples separately. The results demonstrate that uncertainties in the amplitudes do not affect the conclusion of the experiment but do suggest, in addition to the purely statistical error quoted

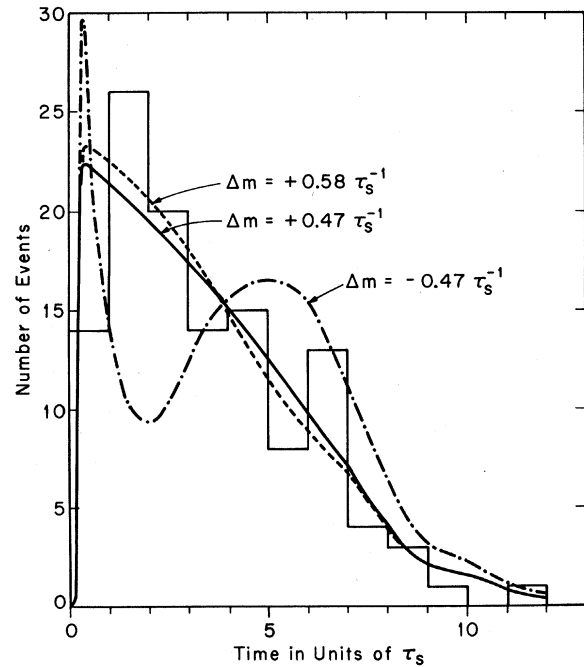


FIG. 9. Observed time distribution for 119 breakup events. Expected distributions for  $|\Delta m| = 0.47\tau_s^{-1}$  are shown along with the expected distribution corresponding to our likelihood best value of  $\Delta m = +0.58\tau_s^{-1}$ .

above, a possible systematic error in  $|\Delta m|$  of the order of  $0.1\tau_S^{-1}$ .

The data have also been analyzed with the magnitude of the mass difference fixed to its known value ( $0.47\tau_S^{-1}$ ). Then the normalized intensities  $I_i(t, +\Delta m)$  and  $I_i(t, -\Delta m)$  for each event were calculated and added to give the expected time distribution for each choice of the sign of  $\Delta m$ . These curves and the observed data are shown in Fig. 9. The  $\chi^2$  probability for  $M_{K_L} > M_{K_S}$  is 0.52 for 7 degrees of freedom, while that for  $M_{K_S} > M_{K_L}$  is less than  $10^{-5}$ . Also shown in Fig. 9 is the expected yield for  $\Delta m = +0.58\tau_S^{-1}$ , which is the value of  $\Delta m$  corresponding to the peak in likelihood function (Fig. 8). The sample was divided according to type of scatter (proton or neutron) and into incident-neutral- $K$  momentum regions. A negative mass difference is rejected when any of these cuts are made on the data.

#### B. Whole-Deuteron Events

Since the amplitudes for  $Kd$  and  $\bar{K}d$  scattering, in the momentum region of interest, have not been experimentally determined, we have constructed these amplitudes using the known  $KN$  and  $\bar{K}N$  scattering amplitudes. Each deuteron amplitude was taken to be a coherent superposition of proton and neutron amplitudes, multiplied by the probability (sticking factor) that the deuteron remain bound. The spin-flip amplitudes must be treated carefully since transitions to the singlet deuteron state are forbidden. After averaging over the initial deuteron spin states and summing over the final state, one finds that the spin-flip terms enter the intensity distribution multiplied by the factor  $\frac{2}{3}$ . Since the data are analyzed using the method of maximum likelihood, the sticking factor need not be calculated since it is a multiplicative factor in the intensity function and therefore cancels in the likelihood function.

A plot of the likelihood function, based upon the 56 deuteron events, is shown in Fig. 10, with the arrow corresponding to the accepted value of  $|\Delta m|$ . We observe a broad peak at  $\Delta m = +0.75$ . We also observe a maximum at  $\Delta m = +2.6$  which is excluded by the  $|\Delta m|$  measurements. While the deuterium data show that  $M_{K_L} > M_{K_S}$ , in agreement with the nucleon data, because of the uncertainty in our method of expressing the  $Kd$  and  $\bar{K}d$  amplitudes, we have not combined the nucleon and deuteron data in a single likelihood analysis.

#### VI. CONCLUSIONS

The result of this experiment is that  $M_{K_L} > M_{K_S}$ . Our result depends only on the broad characteristics (Sec. IV D) concerning the scattering ampli-

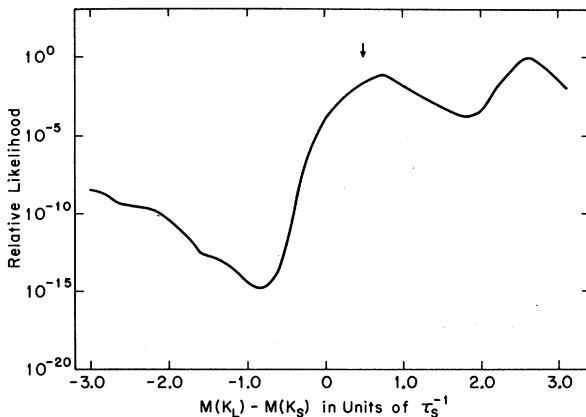


FIG. 10. Plot of the relative likelihood function of  $\Delta m = M(K_L) - M(K_S)$  for 56 whole-deuteron events. The arrow shows the accepted value of  $|\Delta m|$ .

tudes and is not sensitive to the details of the amplitudes. All of these broad characteristics have been established.<sup>20</sup>

The conclusion of this experiment is in agreement with other experiments.<sup>2-4</sup> In the experiment of Mehlhop *et al.*,<sup>2</sup> a neutral- $K$  beam of definite strangeness was produced in a charge-exchange reaction. The interference between regenerated  $K_S^0$  and  $K_S^0$  produced in the original charge-exchange reaction was measured. The interference between these  $K_S^0$  states depends, first, on the proper time between production and regeneration, hence on  $\Delta m$ , and secondly, on the regeneration phase. By studying  $K^\pm$  scattering on the regenerator, in addition to the  $K_S^0$  interference, the sign of  $\Delta m$  was determined to be positive. Kobzarev and Okun<sup>21</sup> had proposed a transmission regeneration method for determining the sign of  $\Delta m$  by observing the interference between coherently regenerated  $K_S^0$  from two different materials. The intensity as a function of regenerator separation is sensitive to  $\Delta m$ . Such an experiment was done by Jovanovich *et al.*<sup>3</sup> using uranium and carbon as the regenerator. An optical-model calculation was necessary to obtain the necessary regeneration phases. Again,  $\Delta m$  was found to be positive. An experiment similar to ours, reported by Meisner *et al.*,<sup>4</sup> also favors  $M_{K_L} > M_{K_S}$ , but with considerably fewer statistics.

#### ACKNOWLEDGMENTS

We thank N. P. Samios for his generous support. We appreciate helpful conversations with L. Wolfenstein and R. Cutkosky. We acknowledge the careful data handling by V. Austen and A. Maxwell. We also wish to thank our scanners, measurers, and the crew of the 30-in. bubble chamber for their efforts.

\*Permanent address: University of Oslo, Blindern, Norway.

†Work supported by the U. S. Atomic Energy Commission.

‡Present address: Tufts University, Medford, Mass.

§Present address: Argonne National Laboratory, Argonne, Ill.

|| Present address: Bettis Atomic Power Laboratory, West Mifflin, Pa.

\*\*Present address: Carnegie-Mellon University, Pittsburgh, Pa.

†† Present address: Digital Equipment Corporation, Maynard, Mass.

§§Work supported by the National Science Foundation.

<sup>1</sup>J. Canter, Y. Cho, A. Engler, H. E. Fisk, R. W. Kraemer, C. M. Meltzer, D. G. Hill, D. K. Robinson, and M. Sakitt, *Phys. Rev. Letters* **17**, 942 (1966).

<sup>2</sup>W. A. W. Mehlhop, S. S. Murty, P. Bowles, T. H. Burnett, R. H. Good, C. H. Holland, O. Piccioni, and R. A. Swanson, *Phys. Rev.* **172**, 1613 (1968).

<sup>3</sup>J. V. Jovanovich, T. Fujii, F. Turkot, G. T. Zorn, and M. Deutsch, *Phys. Rev. Letters* **17**, 1075 (1966).

<sup>4</sup>G. W. Meisner, B. B. Crawford, and F. S. Crawford, Jr., *Phys. Rev. Letters* **17**, 492 (1966).

<sup>5</sup>U. Camerini, W. F. Fry, and J. Gaidos, *Nuovo Cimento* **28**, 1096 (1963).

<sup>6</sup>D. Berley, Alternating Gradient Synchrotron Report No. 25, 1965 (unpublished).

<sup>7</sup>Particle Data Group, *Phys. Letters* **33B**, 11 (1970).

<sup>8</sup>S. Goldhaber, W. Chinowsky, G. Goldhaber, W. Lee, T. O'Halloran, T. F. Stubbs, G. M. Pjerrou, D. H. Stork, and H. K. Ticho, *Phys. Rev. Letters* **9**, 135 (1962).

<sup>9</sup>W. Slater, D. H. Stork, H. K. Ticho, W. Lee, W. Chinowsky, G. Goldhaber, S. Goldhaber, and T. O'Halloran, *Phys. Rev. Letters* **7**, 378 (1961).

<sup>10</sup>V. J. Stenger, W. E. Slater, D. H. Stork, H. K. Ticho, G. Goldhaber, and S. Goldhaber, *Phys. Rev.* **134**, B1111 (1964).

<sup>11</sup>W. E. Humphrey and R. R. Ross, *Phys. Rev.* **127**, 1305

(1962).

<sup>12</sup>M. Sakitt, T. B. Day, R. G. Glasser, N. Seeman, J. Friedman, W. E. Humphrey, and R. R. Ross, *Phys. Rev.* **139**, B719 (1965).

<sup>13</sup>J. K. Kim, *Phys. Rev. Letters* **14**, 29 (1965).

<sup>14</sup>R. Armenteros, P. Baillon, C. Bricman, M. Ferro-Luzzi, D. E. Plane, N. Schmitz, E. Burkhardt, H. Filthuth, E. Kluge, H. Oberlack, R. R. Ross, R. Barloutaud, P. Granet, J. Meyer, J. P. Porte, and J. Prevost, *Nucl. Phys.* **B14**, 91 (1969).

<sup>15</sup>M. B. Watson, M. Ferro-Luzzi, and R. D. Tripp, *Phys. Rev.* **131**, 2248 (1963).

<sup>16</sup>A. K. Ray, R. W. Burris, H. E. Fisk, R. W. Kraemer, D. G. Hill, and M. Sakitt, *Phys. Rev.* **183**, 1183 (1969).

<sup>17</sup>J. A. Kadyk, Y. Oren, G. Goldhaber, S. Goldhaber, and G. H. Trilling, *Phys. Rev. Letters* **17**, 599 (1966).

<sup>18</sup>J. K. Kim, *Phys. Rev. Letters* **19**, 1074 (1967).

<sup>19</sup>M. H. Ross and G. L. Shaw, *Ann. Phys. (N. Y.)* **13**, 147 (1961).

<sup>20</sup>The negative sign of the  $I = 1$   $KN$  amplitude over our momentum range has been determined by Goldhaber *et al.* (Ref. 8). Recently B. Carreras and A. Donnachie [*Nucl. Phys.* **B19**, 349 (1970)] have shown that a single-Regge-pole model for  $KN$  scattering would lead to a solution with positive sign for the amplitude above 1-GeV/ $c$   $K^+$  lab momentum. Using this solution and experimental data, they were able to extend the solution to lower energies and found two possible extensions. One solution remains positive, while the other crosses through zero at about 750 MeV/ $c$  and becomes negative, and is in reasonable agreement with lower-energy  $K^+p$  data. Also, the sign of the real part of the forward  $K^+p$  scattering amplitude is predicted by dispersion relations to be negative and is in reasonable agreement with the data [see, for example, B. R. Martin and G. D. Thompson, *Nucl. Phys.* **B22**, 285 (1970)].

<sup>21</sup>I. Y. Kobzarev and L. B. Okun, *Zh. Eksperim. i Teor. Fiz.* **39**, 605 (1960) [*Soviet Phys. JETP* **12**, 426 (1961)].